

The effect of angle-dependent non-coherent electron scattering and partial redistribution on the polarization of resonance lines

K. E. Rangarajan

Indian Institute of Astrophysics, Bangalore 560034, India

Accepted 1999 May 4. Received 1999 April 12; in original form 1999 January 7

ABSTRACT

The polarized radiative transfer equation is solved when angle-dependent partial redistribution and non-coherent electron scattering are included as line-scattering mechanisms. A static atmosphere with plane parallel symmetry is assumed. Test calculations are used to illustrate the effects of the electron-scattering coefficient, the thermalization parameter and the continuous absorption coefficient on the line polarization. Results of angle-averaged and angle-dependent redistribution functions are compared and it is shown that angle-dependent functions should be used to model the wing polarization of optically thin lines. The lower the continuous absorption compared with the electron scattering, the higher the wing polarization.

Key words: line: formation – polarization – radiative transfer – scattering.

1 INTRODUCTION

Dirac (1925) derived the angle-dependent redistribution function for the electron scattering of low-energy photons ($h\nu < m_e c^2$) taking into account the thermal motion of electrons. He arrived at the conclusion that a shift of the lines cannot be produced by such a scattering mechanism, but broadening of the lines may be possible. He showed that the characteristic width of the redistribution function is 10 \AA for a line formed around $\lambda = 4000 \text{ \AA}$, in an atmosphere of temperature $T = 10^4 \text{ K}$ and at a scattering angle of $\Theta = \pi/2$. The scattering is non-coherent in the observer's frame when the Doppler effect resulting from thermal motion is taken into account. The expression (see equation 16 of this paper) derived by Dirac is especially useful when we remove the restricted assumption of coherent electron scattering in the line-transfer calculations. Such computations may be necessary if the spectrum of the object in question contains features with a width less than or comparable to the electron Doppler width, as in the case of strong lines and continuum edges. In this study we are concerned only with the intensity and polarization of low-energy photons where Compton scattering effects are negligible.

Electron scattering is one of the main sources of opacity in early-type stars and is expected to play an important role in determining the characteristics of spectral lines from their atmospheres. Marlborough (1969) suggested that the broad emission-line wings observed in many Be stars are caused by the electron scattering of line photons, and Bernat & Lambert (1978) concluded that very broad $H\alpha$ emission wings in P Cyg were caused by electron scattering. Castor, Smith & Van Blerkom (1970) showed that non-coherent scattering by free electrons in the WN 6 star HD 192163 can account for the $\lambda 3483$ line of N IV.

The influence of electron scattering in an expanding medium was investigated by Auer & Van Blerkom (1972). They obtained asymmetric line profiles extending preferentially in the red wing. Hillier (1991) made a detailed study of the influence of electron scattering on line profiles arising from stellar winds in early emission-line stars. He found that the use of angle-averaged redistribution functions can noticeably affect the strength of the predicted electron-scattering wings.

1.1 Investigations of line profiles with electron scattering

Münch (1948) considered the case of a semi-infinite atmosphere in which an absorption line is formed, covered by a finite layer of electrons. With these assumptions, he obtained line profiles with shallower cores and broader wings, because the photons are scattered from the continuum into the line core. Auer & Mihalas (1968) gave some solutions to parametrized models in which scattering and absorption in the line, non-coherent electron scattering (NES) and absorption in the continuum all occur simultaneously. They assumed line scattering to be described by the complete redistribution (CRD) mechanism with a Doppler absorption profile, and employed only angle-averaged redistribution functions in their calculations. When the electron-scattering coefficient exceeded the continuous absorption, they obtained measurable changes in the line profile as a result of electron scattering. For strong resonance lines, one has to consider partial frequency redistribution (PRD) of photons by atoms as well as the non-coherent scattering by electrons. Rangarajan, Mohan Rao & Peraiah (1991) studied a few typical samples of PRD cases in which they employed a Voigt absorption profile. Rybicki & Hummer (1994) developed a method to evaluate the

electron-scattering emissivity from a given radiation field and implemented it in their multilevel radiative transfer code (MALI). They investigated the effects arising from the scattering of photons across continuum edges. They showed that in extreme cases this leads to significant shifts of the ionization equilibrium of helium.

1.2 Earlier studies of polarization in lines with electron scattering

Poekert & Marlborough (1978) examined the influence of electron scattering on the Balmer profiles in Be stars and noted that the polarization of the line wings is larger than that of the adjacent continuum. The intrinsic observed polarization of Be stars is typically about 1 per cent at 4000 Å (Poekert, Bastien & Landstreet 1979). Jeffery (1991) has shown that in SN1987A the dominant process determining the polarization structure of the line profiles was electron scattering. Rapid development in the CCD technology now makes it possible to obtain high-quality polarimetric observations across individual lines (Walker et al. 1993). Schulte-Ladbeck et al. (1994) deduced from observations of AG Carinae (a luminous blue variable) that the coexistence of the line-wing polarization with extended flux-line wings was a clear indication that they were formed by electron scattering in a dense wind. Using monochromatic emission, Wood & Brown (1994) showed that the scattered polarimetric profile contains information on the density and velocity structure of the circumstellar disc. Recently, Hillier (1996) investigated the polarized line profiles in stars with extended and expanding envelopes, but with a restriction that the polarization arises entirely from electron scattering. Even though Nagendra, Rangarajan & Mohan Rao (1993) considered the scattering of photons by both atoms and electrons in their parametric study, they employed only angle-averaged expressions in their calculations.

Most of the above-mentioned studies are restricted to single-scattering approximations or the angle-averaged expressions in the scattering functions. One of the main aims of this study is to investigate the differences in polarization results when angle-averaged redistribution functions are used in the calculations compared with the results obtained using angle-dependent functions. We employ the angle-dependent functions for the scattering by atoms (PRD) and non-coherent electron scattering (NES) and solve the radiative transfer equation in the Stokes vector formalism for a static medium with plane parallel symmetry. A parametric study is made so that the underlying physics can be discerned. In Section 2 the relevant equations are described. In Section 3 the results of the computations are presented and discussed. Finally, in Section 4 the conclusions are given.

2 POLARIZED LINE-TRANSFER EQUATION WITH ELECTRON SCATTERING

In a non-magnetic plane-parallel atmosphere with azimuthal symmetry in the radiation field, it is sufficient to consider the Stokes parameters I_l and I_r to represent the polarization state of the radiation field. The total intensity is defined as $I = I_l + I_r$ and the Stokes Q parameter is defined as $Q = I_l - I_r$. As in Chandrasekhar (1960), I_l and I_r denote the intensities of linearly polarized radiation along two perpendicular directions l and r . The

linear polarization is defined as $p = (Q/I)$. With the above definitions, the vector transfer equation for a two-level atom becomes

$$\mu \frac{d\mathbf{I}(x, \mu, z)}{dz} = -\chi(x, \mu, z)\mathbf{I}(x, \mu, z) + \boldsymbol{\eta}(x, \mu, z). \quad (1)$$

Here $\mathbf{I} = (I_l, I_r)^T$ and $\boldsymbol{\eta}$ is the emission coefficient. The total absorption coefficient is given by

$$\chi(x, \mu, z) = \chi_l(z)\phi(x, z) + \chi_c(x, \mu, z) + \chi_e(x, \mu, z). \quad (2)$$

In equation (2), χ_c , χ_l and χ_e are the coefficients of continuous absorption, atomic absorption and electron scattering at the line centre respectively. $\chi^e = N_e \sigma_e$ where σ_e is Thomson scattering coefficient and N_e the electron number density). ν_0 is the line centre frequency. The optical depth scale is defined as $d\tau(z) = -\chi_l(z) dz$. The symbol μ denotes $\cos(\theta)$ where θ is the angle made by the ray with the normal to the surface. It is convenient to measure the frequency displacements from the line centre in units of Doppler width $\Delta\nu_D = \nu_0 v_{th}/c$, where v_{th} is the thermal velocity:

$$x = \frac{\nu - \nu_0}{\Delta\nu_D}, \quad \text{with } \Delta\nu_D = \frac{\nu_0}{c} \sqrt{\frac{2kT}{m}}. \quad (3)$$

The constants c and k are the velocity of light and the Boltzmann constant. m is the mass of the atom under consideration. We have used a Voigt function with a depth-independent damping parameter as the absorption profile throughout this study, and it is denoted by

$$\phi(x) = \frac{1}{\sqrt{\pi}} H(a, x), \quad (4)$$

where the Voigt parameter a represents a constant ratio of the damping width to the Doppler width. The emission coefficient is defined analogously as

$$\boldsymbol{\eta}(x, \mu, z) = \boldsymbol{\eta}_l(x, \mu, z) + \boldsymbol{\eta}_c(x, \mu, z) + \boldsymbol{\eta}_e(x, \mu, z), \quad (5)$$

with the subscripts ‘l’, ‘c’ and ‘e’ indicating line, continuum and electrons respectively. The total source function $\mathbf{S}_{tot}(x, \mu, z)$ is given by

$$\begin{aligned} \mathbf{S}_{tot}(x, \mu, z) &= \frac{\boldsymbol{\eta}(x, \mu, z)}{\chi(x, \mu, z)} \\ &= \frac{\mathbf{S}_l(x, \mu, z)\phi(x) + \mathbf{S}_c[\chi_c/\chi_l] + \mathbf{S}_e(x, \mu, z)[\chi_e/\chi_l]}{\phi(x) + [\chi_c/\chi_l] + [\chi_e/\chi_l]}. \end{aligned} \quad (6)$$

Defining the continuum atomic absorption parameter as $\beta_c = [\chi_c/\chi_l]$, and the continuum electron scattering parameter as $\beta_e = [\chi_e/\chi_l]$, we can rewrite equation (6) as

$$\mathbf{S}_{tot}(x, \mu, z) = \frac{\phi(x)\mathbf{S}_l(x, \mu, z) + \beta_c\mathbf{S}_c + \beta_e\mathbf{S}_e(x, \mu, z)}{\phi(x) + \beta_c + \beta_e}, \quad (7)$$

where the continuum source function \mathbf{S}_c is defined as

$$\mathbf{S}_c = \frac{1}{2}B(z)\mathbf{1} = \frac{1}{2}\mathbf{B}\mathbf{1}; \quad \mathbf{1} = [11]^T. \quad (8)$$

We have considered only isothermal, static atmospheres in this study. Consequently β_c and β_e are constant throughout the atmosphere. However it is straightforward to consider the dependence of these variables on all the physical and geometric

parameters. The two-level atom line-source vector is given by

$$\mathbf{S}_1(x, \mu, z) = \begin{pmatrix} S_1^l(x, \mu, z) \\ S_1^r(x, \mu, z) \end{pmatrix} = \frac{(1 - \epsilon)}{\phi(x)} \int_{-\infty}^{+\infty} dx' \times \int_{-1}^{+1} \mathbf{R}^a(x, \mu, x', \mu') \mathbf{I}(x', \mu', z) d\mu' + \frac{\epsilon}{2} \mathbf{B}\mathbf{1}, \quad (9)$$

where ϵ is the probability per scatter that a photon is destroyed by collisional de-excitation. The redistribution matrix $\mathbf{R}^a(x, \mu, x', \mu')$ accounts for the correlations in frequency, angle and polarization state that exist between the incident photon characterized by (x, μ) and the re-emitted photon characterized by (x', μ') during a scattering event involving a two-level atom and the incident and re-emitted photons. This matrix is normally approximated for scattering on a two-level atom, in the form

$$\mathbf{R}^a(x, \mu, x', \mu') = \mathbf{P}^a(\mu, \mu') \mathbf{R}^a(x, x'), \quad (10)$$

whereas in this study we use the full angle-dependent redistribution matrix defined by

$$R^a(x, \mu, x', \mu') = \frac{1}{2\pi} \int_0^{2\pi} \mathbf{P}^a(\mathbf{n}, \mathbf{n}') R(x, x', \gamma) d\Delta, \quad (11)$$

with

$$R(x, x', \gamma) = \frac{1}{\pi |\sin \gamma|} \exp \left[- \left(\frac{x' - x}{2 \sin \gamma/2} \right)^2 \right] \times H \left[\frac{a}{\cos(\gamma/2)}; \frac{x + x'}{2 \cos(\gamma/2)} \right], \quad (12)$$

γ being the angle between \mathbf{n} and \mathbf{n}' . The above expression is the well-known type II redistribution function of Hummer (1962), which refers to the case of a two-level atom, the upper level of which is naturally broadened, with the lower level having zero width. $\mathbf{P}^a(\mathbf{n}, \mathbf{n}')$ is the angular phase matrix for resonance scattering (Chandrasekhar 1960) in the base (I_l, I_r) , which is a function of μ, μ' and $\Delta = \phi' - \phi$, the difference of azimuthal directions of the incident and re-emitted radiation fields. The relation between γ and these quantities is $\cos \gamma = \mu\mu' + \sqrt{(1 - \mu^2)(1 - \mu'^2)} \cos \Delta$. The angular phase matrix for resonance scattering is defined by

$$\mathbf{P}^a(\mu, \mu') = \frac{3}{2} E_1 \begin{pmatrix} (l, l)^2 & (r, l)^2 \\ (l, r)^2 & (r, r)^2 \end{pmatrix} + \frac{(1 - E_1)}{2} \begin{pmatrix} 1 & 1 \\ 1 & 1 \end{pmatrix}, \quad (13)$$

where

$$(l, l) = (1 - \mu'^2)^{1/2} (1 - \mu^2)^{1/2} + \mu' \mu \cos \Delta, \\ (r, l) = \mu \sin \Delta, \quad (14)$$

$$(l, r) = -\mu' \sin \Delta, \quad (r, r) = \cos \Delta.$$

The factor $(1 - E_1)$ measures the amount of atomic depolarization. E_1 depends on the angular momentum quantum numbers j_l and j_u of the transition involved (l = lower state and u = upper state). A maximum polarization occurs for the $(j_l = 0) \rightarrow (j_u = 1)$ type of transition, when $E_1 = 1$. In this special case, $\mathbf{P}^a(\mu, \mu')$ reduces to the classical Rayleigh scattering phase matrix. Analogously the electron-scattering source function $\mathbf{S}_e(x, \mu, z)$ is given by

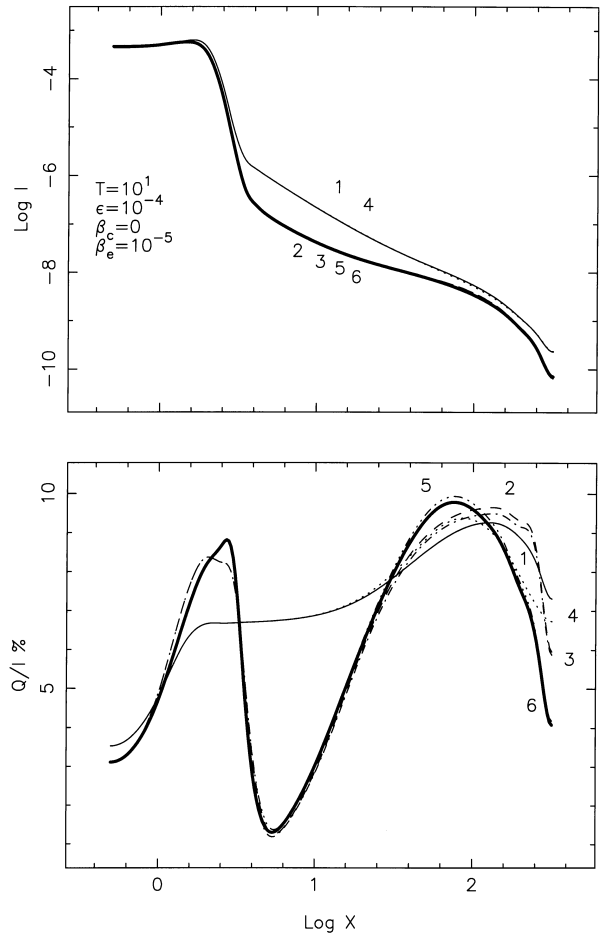


Figure 1. Emergent intensities $I(\tau = 0, x, \mu_1)$ and polarization Q/I per cent in the direction $\mu_1 = 0.11$ for the given model represented by $(T, \epsilon, \beta_c, \beta_e)$. The abscissa gives the frequency x measured from the line centre in the units of atomic Doppler width. Curves 1–3 show the results for angle-averaged non-coherent electron scattering (AA-NES) and curves 4–6 represent the results for angle-dependent non-coherent electron scattering (AD-NES). Curves 1 (thin solid line), and 4 (dotted line) indicate the results for complete redistribution (CRD) of photons by atoms, curves 2 (thin-dashed line) and 5 (dash followed by triple dots) represent the angle-averaged partial redistribution by atoms (AA-PRD) and curves 3 (thin dash-dotted line) and 6 (thick solid line) give the results for angle-dependent partial redistribution (AD-PRD) by atoms. The medium is an optically thin, isothermal, self-emitting slab with total optical depth at the line centre $T = 10^1$.

$$\mathbf{S}_e(x, \mu, z) = \begin{pmatrix} S_e^l(x, \mu, z) \\ S_e^r(x, \mu, z) \end{pmatrix} = \int_{-\infty}^{+\infty} dx' \int_{-1}^{+1} \mathbf{R}^e(x, \mu, x', \mu') \mathbf{I}(x', \mu', z) d\mu'. \quad (15)$$

The expression for the angular phase matrix of the electron scattering is obtained from equation (13) by taking $E_1 = 1$. The angle-dependent redistribution function for electron scattering in the laboratory frame is given by (Mihalas 1978)

$$R^e(\nu', \mathbf{n}', \nu, \mathbf{n}) = \left[\frac{mc^2}{4\pi kT(1 - \cos \Theta)\nu^2} \right]^{1/2} \times \exp \left[\frac{-mc^2(\nu - \nu')^2}{4kT(1 - \cos \Theta)\nu^2} \right]. \quad (16)$$

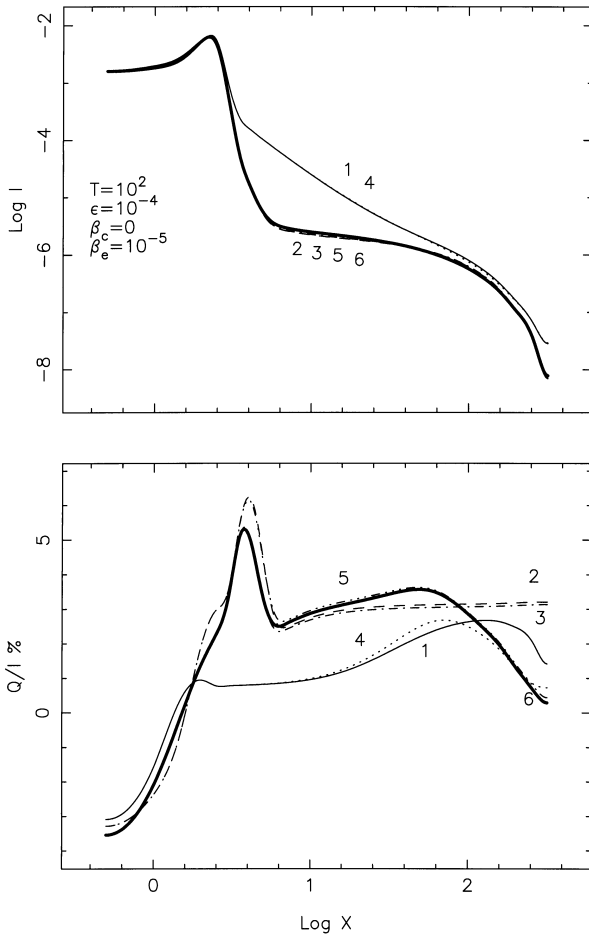


Figure 2. Same as Fig. 1, but for a medium with optical depth $T = 10^2$.

Now $\omega = x\Delta\nu_c/(\nu - \nu_0)$, where ω is the ratio of electron to atomic Doppler widths and is given by $\omega \approx 43A^{1/2}$, where A is the atomic weight of the atom under consideration. For helium atoms, ω is nearly equal to 80.

2.1 Computational procedure

Discrete space theory technique (Grant & Hunt 1969) was used to solve the transfer equation. The computational time of this technique scales linearly (approximately) with the number of frequency points. The memory requirements, however, are large because the reflection and transmission matrices (size of a matrix = number of frequency points \times number of angles \times number of Stokes parameters) have to be stored at each layer of the atmosphere. The electron scattering makes significant contributions only in the far wings. Hence, in order to perform accurate transfer calculations it is necessary to select a very wide frequency band ($x_{\max} \sim 300\text{--}400$) and, correspondingly, a large number of frequency points. In practical terms, it becomes computationally expensive to deal with this problem. The total half-bandwidth selected is approximately four electron Doppler widths for a He atom, which corresponds to 320 atomic Doppler widths. For frequency integrations, a 29-point frequency quadrature is employed between $x = 0$ and $x = 360$. For angular integrations a three-point Gaussian quadrature is employed in the range $\mu \in (0, 1)$. The scattering integral over the atomic redistribution function $R_{ij}^a(x, \mu; x', \mu')$ and the electron redistribution

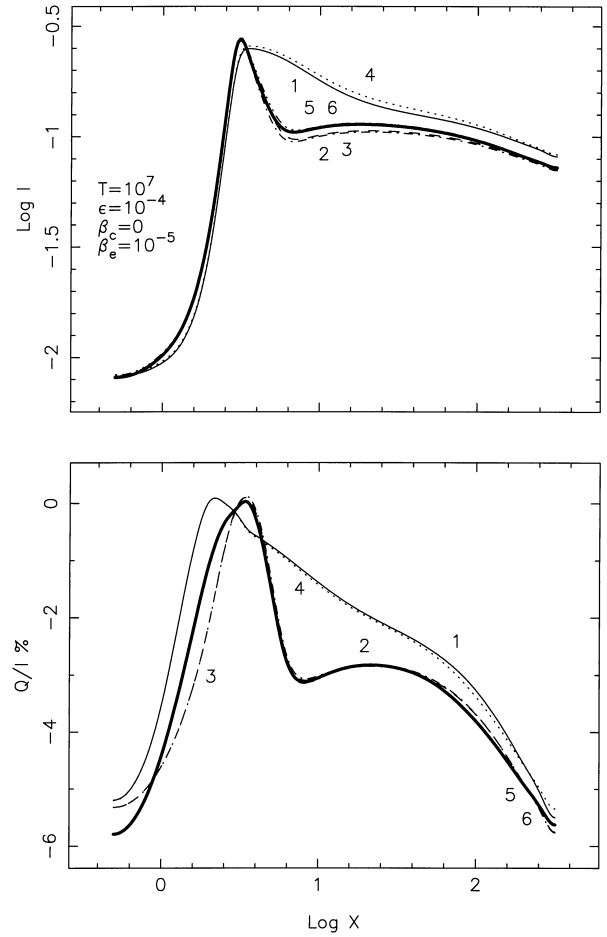


Figure 3. Same as Fig. 1, but for an optically thick medium with $T = 10^7$. The medium is irradiated at one of the boundaries with $I(\tau = T, x, \mu) = 1$. In all the subsequent figures the optically thick medium is always irradiated in the same way.

function $R^e(x, \mu; x', \mu')$ are performed by a natural cubic-spline representation of the radiation field (the algorithm of Adams, Hummer & Rybicki 1971). In the angle-dependent functions, the integration over the azimuthal angle is computed with a 10-point Gaussian quadrature formula on the interval $0 < \Delta < \pi$. The code was tested for the angle-dependent PRD cases, when electron scattering was absent ($\beta_e = 0$), against the results of Faurobert (1987). The intensity and polarization profiles obtained by us were found to be in good agreement with the published graphs of Faurobert.

3 RESULTS AND DISCUSSION

We considered two types of atmospheres. One is an optically thin medium where the primary sources of radiation are inside the atmosphere. This is also referred to as the ‘self-emitting slab’. The boundary conditions for a finite slab of optical thickness T are

$$I(x, \mu, \tau = T) = I(x, -\mu, \tau = 0) = 0, \quad (17)$$

The other type of atmosphere is an optically thick medium with $T = 10^7$, and the boundary conditions chosen to mimic the typical stellar atmosphere are

$$I(x, \mu, \tau = T) = B \quad \text{and} \quad I(x, -\mu, \tau = 0) = 0, \quad (18)$$

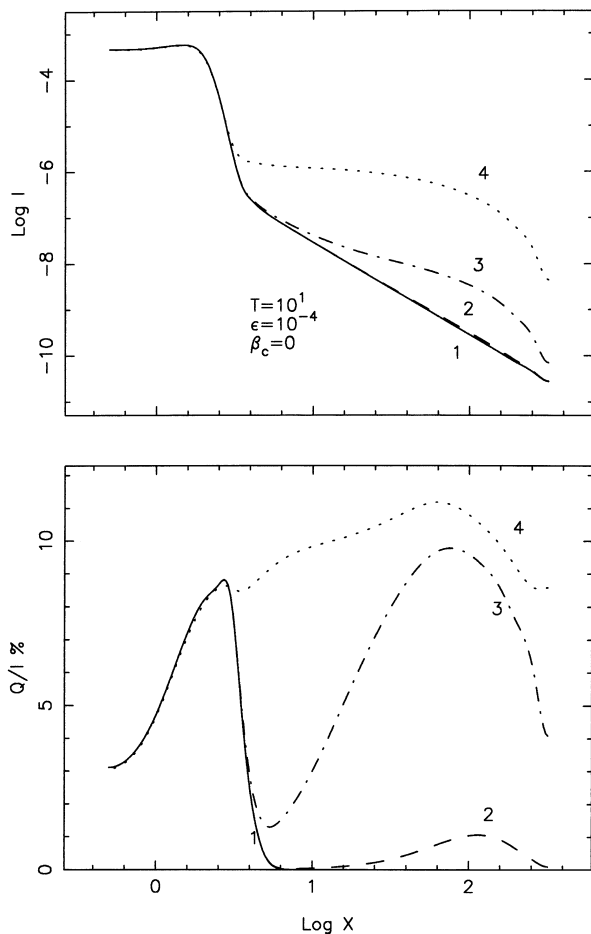


Figure 4. The figure shows the effect of varying the electron scattering contribution to the opacity for optically thin lines. The solid line (curve 1) represents the results for the case when no electron scattering is present, $\beta_e = 0$. The dashed line (curve 2) gives the results for a medium with $\beta_e = 10^{-7}$, the dash-dotted line (curve 3) represents the results for $\beta_e = 10^{-5}$, and the dotted line (curve 4) indicates the results for $\beta_e = 10^{-3}$.

Calculations have been performed with the depth-independent values of the probability of collisional destruction ϵ and the Planck function B . The natural width of the upper level, denoted by a , is 10^{-3} in units of Doppler width, and $B = 1$. Most of the results are compared with a standard model, the parameters of which are $\epsilon = 10^{-4}$, $\beta_c = 0$ and $\beta_e = 10^{-5}$, where angle-dependent PRD and NES functions are employed. For the sake of convenience we have shown the logarithm of frequency on the x -axis. The ordinates refer to $\log I(x, \mu = 0.11, \tau = 0)$, and to the percentage of emergent linear polarization $p(x, \mu = 0.11, \tau = 0)$ in the upper and lower halves of all the figures respectively.

3.1 Comparison between angle-dependent and angle-averaged electron redistribution

We have illustrated the differences between angle-averaged and angle-dependent electron-scattering results in Figs 1–3. In studying these figures, one has to bear in mind that there are two different scattering mechanisms operating on line photons; one is caused by atoms and the other by electrons. The comparison between angle-averaged electron redistribution and angle-dependent electron redistribution will be valid only if we keep the

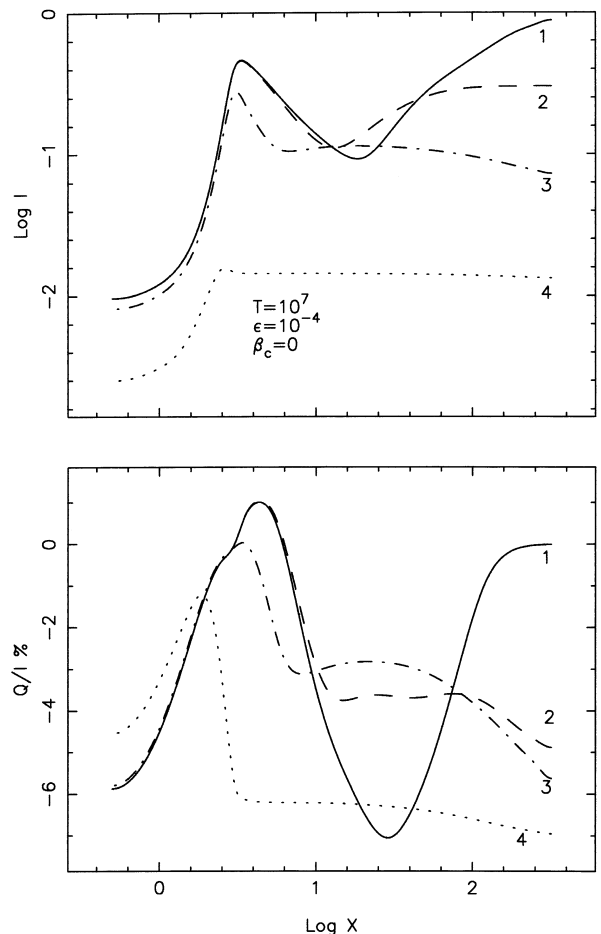


Figure 5. Same as Fig. 4, but for an optically thick medium with $T = 10^7$.

atomic redistribution the same for both cases. In all the figures, curves 1 and 4 represent CRD cases with angle-averaged and angle-dependent electron redistributions, respectively. Similarly, curves 2 and 5 show the angle-averaged PRD cases and curves 3 and 6 the angle-dependent PRD cases. We see from Figs 1 and 2 that for optically thin cases, even though the angle-dependent and angle-averaged electron-scattering polarization results are in qualitative agreement, there is a considerable difference between them quantitatively in the wings (nearly 2 per cent polarization in the far wings).

Therefore, when modelling the wing polarization in optically thin lines, one has to use angle-dependent non-coherent electron scattering. This may be understood as follows. For optically thin lines, the single-scattering approximation is valid in the wings and the single scattering is sensitive to angular effects. As one increases the optical depth, one can expect multiple scattering to take place, which averages out the angle-dependent effects. This is what we find when we look at Figs 2 and 3. We see that even the quantitative differences between the angle-dependent and angle-averaged NES results have been reduced in Fig. 2 and are almost absent in Fig. 3. Polarization is a measure of anisotropy. Anisotropy depends on the angular dependence present in the scattering. Therefore polarization is more sensitive to angle-dependent expressions, in comparison with the total specific intensity. Again, if we have velocities present in the medium, they will couple with the angular dependence of the scattering mechanism and produce quite characteristic polarization results.

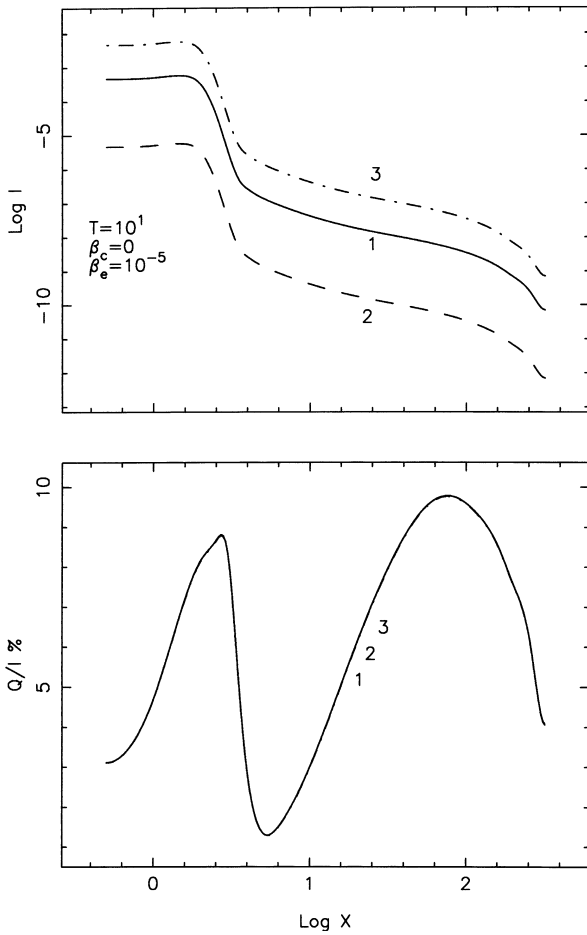


Figure 6. The figure shows the effect of varying the thermal contribution (ϵ). The solid line (curve 1) represents the results for the case when the thermalization parameter is $\epsilon = 10^{-4}$. The dashed line (curve 2) gives the results for a medium with $\epsilon = 10^{-6}$, and the dash-dotted line (curve 3) represents the results for $\epsilon = 10^{-3}$.

The polarization profiles 1 and 4 for an optically thin medium ($T = 10$), correspond to CRD results, and they show small polarization in the line core followed by uniformly high polarization in the wings. Fractional polarization in the optically thin wings is given by Faurobert (1987):

$$p(x, \mu) \approx \frac{S_Q(T/2, x, \mu)}{S_I(T/2, x, \mu)}. \quad (19)$$

From the above expression it can be seen that for CRD, the polarization stays constant in the optically thin wings at a value that depends on the anisotropy of the radiation field at the slab centre. It decreases when the total optical thickness of the medium increases (compare Fig. 2 with Fig. 1). For frequencies less than $x = 10$, the atomic redistribution dominates, and the PRD allows lesser scatterings and hence higher anisotropy, which leads to a polarization maximum. Around $x = 10$, the scattering term resulting from PRD reduces and the radiation field is dominated by thermal photons, which are isotropic; hence we obtain a polarization minimum. Beyond $x = 10$, we find the NES dominates, giving rise to a substantial polarization. One important result that emerges is that whatever the atomic scattering mechanism, the electron scattering gives substantial polarization in the wings of optically thick lines (Fig. 3).

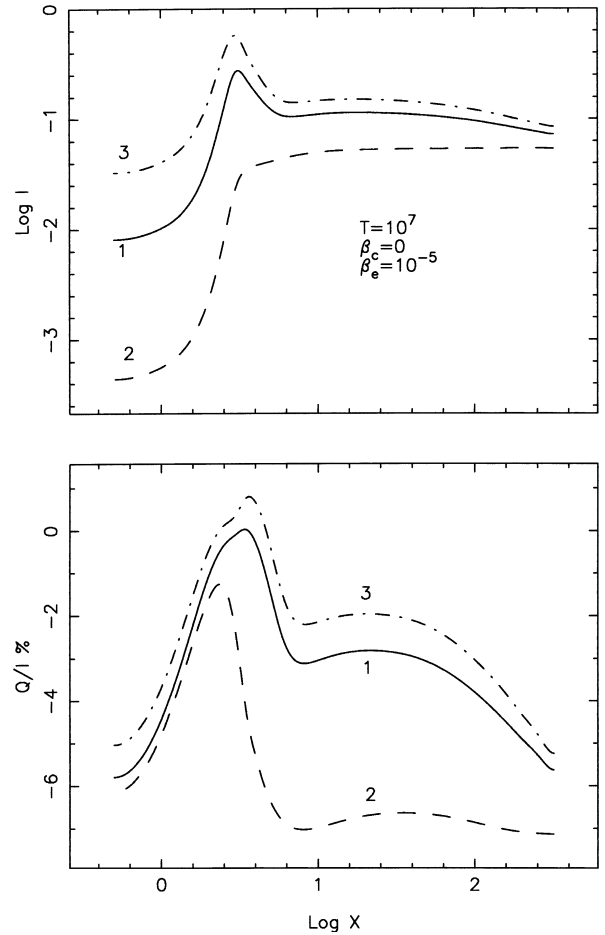


Figure 7. Same as Fig. 6, but for an optically thick medium with $T = 10^7$.

3.2 Effects of β_e on polarization

The effects of β_e variation on polarization for various types of atmospheres are shown in Figs 4 and 5. In these models, we have used both angle-dependent PRD and angle-dependent NES as scattering mechanisms. We find that when the electron-scattering contribution is increased, the minimum polarization observed around $x = 8$ is shifted in frequency towards the centre and its absolute value also changes. We find from these figures that higher electron-scattering contribution gives higher polarization in the wings, irrespective of the optical depth of the medium. The minimum and maximum values attained in polarization seem to be a sensitive indicator of β_e .

3.3 Effect of ϵ variation

The effect of varying ϵ is shown in Figs 6 and 7. For an optically thin medium (Fig. 6), we find that the parameter ϵ does not have any effect on polarization. The wing polarization depends on the anisotropy present in the centre of the medium. Anisotropy present in the centre of the slab depends only on optical depth and not on ϵ . To obtain the intensity, one has to integrate the thermal contributions over the whole medium, which gives a substantial change in intensity for different ϵ values. For an optically thick atmosphere, the contribution to the wing photons from scattering is less in comparison with thermal contributions. Photons from the

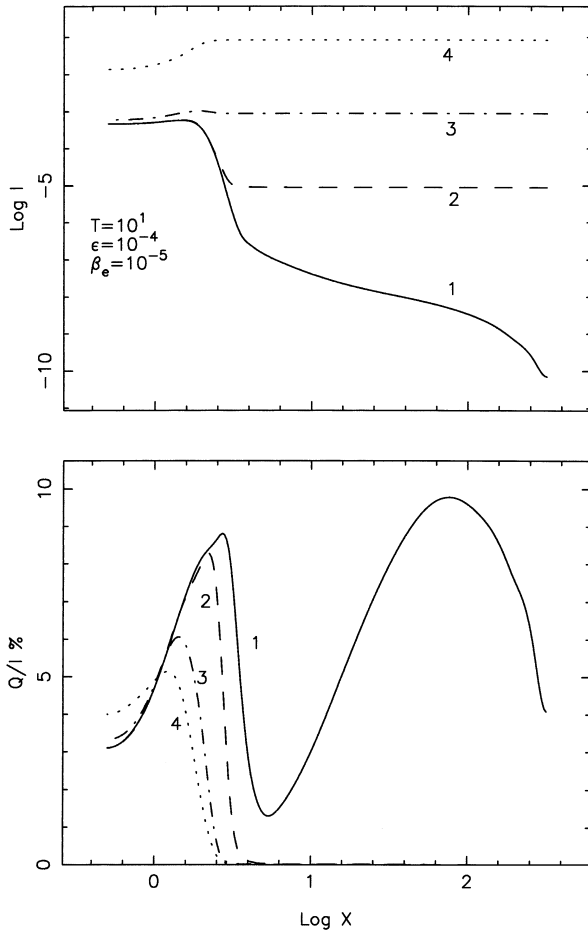


Figure 8. The figure shows the effect of varying the continuous absorption contribution to the opacity for optically thin lines. The solid line (curve 1) represents the results for the case when no continuous absorption is present ($\beta_c = 0$). The dashed line (curve 2) gives the results for a medium with $\beta_c = 10^{-7}$, the dash-dotted line (curve 3) represents the results for $\beta_c = 10^{-5}$, and the dotted line (curve 4) indicates the results for $\beta_c = 10^{-3}$.

thermal pool are isotropic, and hence the higher thermalization parameter gives lower polarization (Fig. 7).

3.4 Effect of variation of continuous absorption β_c on polarization

The effect of varying β_c on polarization is shown in Figs 8 and 9. The continuous absorption and emission are the important physical processes in the optically thin line wings (Fig. 8). The continuous absorption is assumed to be isotropic. It therefore produces zero polarization in the wings for an optically thin line. One interesting result is that the core polarization is sensitive to the continuous absorption for optically thin lines. The continuous absorption and electron scattering seem to play opposite roles in polarizing the radiation for optically thick lines. When $\beta_c = \beta_e$, the polarization flips in sign in the wing for an optically thick line. When β_c exceeds β_e (see curve 4 of Fig. 9) it produces zero polarization in the wing of an optically thick line. Hence we cannot say that the wing polarization of optically thick lines is a monotonic function of β_c/β_e .

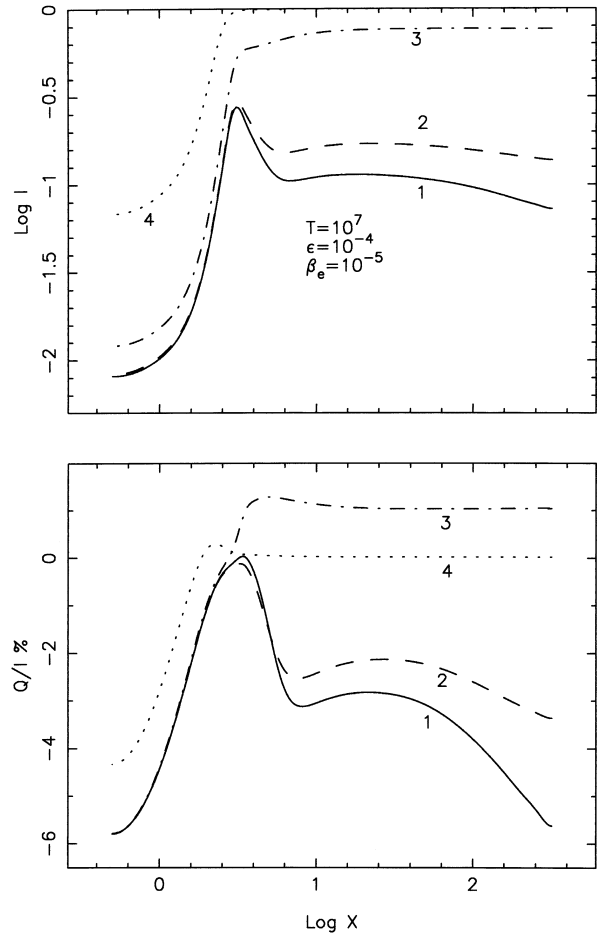


Figure 9. Same as Fig. 8, but for an optically thick medium with $T = 10^7$.

4 CONCLUSIONS

We find quantitative differences in the wing polarization of optically thin lines, when we compare the results of angle-dependent NES with those of angle-averaged NES. The differences in the results of these functions may be enhanced if velocities are present in the medium. A systematic study should be undertaken to ascertain the validity of using angle-averaged NES expressions for calculating the polarization in the above case. Polarization is not affected by the thermalization parameter for optically thin lines, and it is completely controlled by purely β_e . When electron scattering is greater than continuous absorption, it produces wing polarization in optically thick lines, and this fact may be used as a diagnostic tool.

ACKNOWLEDGMENTS

I thank Professor George Rybicki for suggesting the problem and helpful discussions. I am indebted to Dr M. Faurobert-Scholl for providing a program to compute the angle-dependent redistribution function $R^a(x, \mu; x', \mu')$ and Mr B. A. Varghese for his help in creating the figures shown in this paper. The useful suggestions made by the anonymous referee have improved the text of the paper considerably, and I thank the referee for that.

REFERENCES

- Adams J. F., Hummer D. G., Rybicki G. B., 1971, *J. Quant. Spectrosc. Radiat. Transfer.*, 11, 1365
- Auer L. H., Mihalas D., 1968, *ApJ*, 153, 245
- Auer L. H., Van Blerkom D., 1972, *ApJ*, 178, 175
- Bernat A. P., Lambert D. L., 1978, *PASP*, 90, 520
- Castor J. I., Smith L. F., Van Blerkom D., 1970, *ApJ*, 159, 1119
- Chandrasekhar S., 1960, *Radiative Transfer*, Oxford Univ. Press, Oxford
- Dirac P. A. M., 1925, *MNRAS*, 85, 825
- Faurobert M., 1987, *A&A*, 178, 269
- Grant I. P., Hunt G. E., 1969, *Proc. R. Soc. London, Ser. A.*, 313, 183
- Hillier D. J., 1991, *A&A*, 247, 455
- Hillier D. J., 1996, *A&A*, 308, 521
- Hummer D. J., 1962, *MNRAS*, 125, 21
- Jeffery D. J., 1991, *ApJ*, 375, 264
- Marlborough J. M., 1969, *ApJ*, 156, 135
- Mihalas D., 1978, *Stellar Atmospheres*, Freeman, San Francisco
- Münch G., 1948, *ApJ*, 108, 116
- Nagendra K. N., Rangarajan K. E., Mohan Rao D., 1993, *MNRAS*, 262, 855
- Poeckert R., Marlborough J. M., 1978, *ApJS*, 38, 229
- Poeckert R., Bastien P., Landstreet J. D., 1979, *AJ*, 84, 812
- Rangarajan K. E., Mohan Rao D., Peraiah A., 1991, *MNRAS*, 250, 633
- Rybicki G. B., Hummer D. G., 1994, *A&A*, 290, 553
- Schulte-Ladbeck R. E., Clayton G. C., Hillier D. J., Harries T. J., Howarth I. D., 1994, *ApJ*, 429, 846
- Walker G., Dinshaw N., Saddlemyer L., Younger F., 1993, *Exp. Astron.*, 2, 391
- Wood K., Brown J. C., 1994, *A&A*, 285, 220

This paper has been typeset from a $\text{\TeX}/\text{\LaTeX}$ file prepared by the author.